Revue des Composites et des Matériaux Avancés-Journal of Composite and Advanced Materials
Vol. 35, No. 4, August, 2025, pp. 747-753
Journal homepage: http://iieta.org/journals/rcma

Optimizing Lead-Free Cs_2NaBiI_6 Perovskite Solar Cells via Mg^{2+} Doping: Enhanced Efficiency and Stability

Arkan G. Salman*, Majid R. Al-Bahrani

Laboratory of Nanomaterials and Plasma, College of Science, University of Thi-Qar, Nasiriyah 64001, Iraq

Corresponding Author Email: arkan.salman@utq.edu.iq

https://doi.org/10.18280/rcma.350416

Received: 15 July 2025
Revised: 16 August 2025
Accepted: 25 August 2025
Available online: 31 August 2025

Keywords:
lead-free perovskite, Cs_2NaBiI_6, magnesium doping, double perovskite, eco-friendly solar cells, optoelectronic properties

ABSTRACT

Lead-free halide double perovskites are promising alternatives to toxic lead-based counterparts owing to their environmental stability and benign composition. Among these, iodide-based Cs_2NaBiI_6 has attracted attention due to its narrower bandgap (~1.6–1.8 eV) compared to bromide analogues such as $Cs_2AgBiBr_6$ (~2.0 eV), making it more suitable for solar harvesting. However, limited studies have addressed strategies to enhance its optoelectronic performance. In this work, we systematically investigate the effect of Mg^{2+} incorporation on the structural, morphological, optical, and photovoltaic properties of Cs_2NaBiI_6 thin films and devices. X-ray diffraction (XRD) and FE-SEM analyses reveal that moderate Mg^{2+} doping (3%) improves crystallinity and film compactness, leading to enhanced optical absorption and reduced bandgap (~1.65 eV). Photovoltaic measurements across 100 devices (25 per group) demonstrate a reproducible improvement in power conversion efficiency from 0.62% (pristine) to 1.22% (3% Mg^{2+}), primarily due to increased short-circuit current density and fill factor. At higher doping (5%), performance degrades, consistent with structural disorder and morphological irregularities. Although the overall efficiency remains modest compared to Pb-based perovskites, Mg^{2+}-doped Cs_2NaBiI_6 exhibits superior environmental stability and reproducibility, suggesting its potential for niche applications such as indoor photovoltaics and long-lifetime devices. These findings highlight the viability of cation doping as an effective approach to tune the optoelectronic properties of iodide-based lead-free double perovskites.

1. INTRODUCTION

Lead halide perovskites have attracted enormous interest in recent years owing to their exceptional optoelectronic properties [1-3], including high absorption coefficients, long carrier diffusion lengths, and tunable bandgaps [4-7]. Despite these advantages, the presence of toxic lead and the limited long-term stability of lead-based perovskites remain critical obstacles to large-scale commercialization. To overcome these issues, considerable effort has been devoted to the exploration of lead-free double perovskites with the general formula $A_2B(I)B(III)X_6$, where A is a monovalent cation (e.g., Cs^+), B(I) is a monovalent metal (e.g., Na^+, Ag^+), B(III) is a trivalent cation (e.g., Bi^{3+}, Sb^{3+}), and X is a halide anion (Cl^-, Br^-, I^-) [8-12]. These materials offer improved environmental stability and reduced toxicity compared to Pb-based analogues, though their optoelectronic performance still requires significant enhancement.

Among lead-free double perovskites, bromide-based compounds such as $Cs_2AgBiBr_6$ have been extensively studied due to their structural stability and defect tolerance [8]. However, their relatively wide bandgap (~2.0 eV) limits light-harvesting capability under the solar spectrum, resulting in modest photovoltaic efficiencies. In contrast, iodide-based double perovskites such as Cs_2NaBiI_6 possess a narrower optical bandgap (~1.6-1.8 eV), which is closer to the optimum range for solar energy conversion [13]. Nevertheless, research on iodide-based double perovskites remains limited compared to their bromide counterparts, and strategies to optimize their optoelectronic properties are still underexplored.

One promising approach to tuning the structural and electronic properties of double perovskites is cation doping. Incorporating aliovalent or isovalent dopants can modify lattice parameters, reduce defect density, and improve charge transport pathways [14]. Magnesium (Mg^{2+}), with its smaller ionic radius relative to Na^+ or Bi^{3+}, is particularly interesting since it can induce slight lattice distortion, enhance orbital overlap, and reduce trap states, thereby narrowing the bandgap and potentially improving carrier dynamics [15, 16]. While Mg^{2+} doping has been previously investigated in $Cs_2AgBiBr_6$, its influence on iodide-based Cs_2NaBiI_6 remains largely unexplored [17, 18]. Understanding how Mg^{2+} incorporation affects the crystallinity, morphology, optical absorption, and photovoltaic performance of Cs_2NaBiI_6 is therefore of significant importance.

In this work, we systematically investigate the effect of Mg^{2+} doping on the structural, morphological, optical, photovoltaic properties of Cs_2NaBiI_6 thin films, and devices. We show that moderate Mg^{2+} incorporation improves film crystallinity, grain connectivity, and optical absorption while maintaining the inherent environmental stability of Cs_2NaBiI_6. Although the achieved power conversion efficiency (1.22%) is modest compared to state-of-the-art lead halide perovskites, the excellent stability and reproducibility (25 devices per group, 100 devices in total) highlight the potential of Mg^{2+}-doped Cs_2NaBiI_6 for niche applications such as indoor photovoltaics or long-lifetime devices, where stability is more critical than peak efficiency. We further contextualize our results by comparing them with recent studies (2023-2024) on stability enhancement strategies in lead-free perovskites, including interface passivation [19-22], dimensional engineering [23-25], and defect management, thereby providing a comprehensive framework for future development of environmentally benign perovskite materials.

2. MATERIALS AND METHODS

2.1 Materials

All precursor materials were of analytical grade and used as received without further purification. Cesium iodide (CsI, 99.9%), sodium iodide (NaI, 99.9%), bismuth iodide (BiI_3, 99.9%), and magnesium iodide (MgI_2, 99.9%) were obtained from Sigma-Aldrich. Zinc oxide (ZnO) nanoparticle dispersion and nickel oxide (NiO) nanoparticle solution were purchased from commercial suppliers and used for the electron transport layer (ETL) and hole transport layer (HTL), respectively. Dimethyl sulfoxide (DMSO) and dimethylformamide (DMF) were used as solvents. All solutions were prepared in a nitrogen-filled glovebox under controlled humidity (<1% RH).

2.2 Film preparation

The Cs_2NaBiI_6 perovskite precursor solution was prepared by dissolving stoichiometric amounts of CsI, NaI, and BiI_3 in a DMSO/DMF solvent mixture under continuous stirring at 60°C. For Mg^{2+}-doped samples, MgI_2 was introduced at different molar ratios (1%, 3%, and 5%) relative to the Na^+ site, while the undoped composition was used as a reference. The solutions were filtered (0.45 μm PTFE) before deposition.

Perovskite thin films were deposited on pre-cleaned FTO-coated glass substrates. The substrates were sequentially ultrasonicated in acetone, isopropanol, and deionized water, followed by UV–ozone treatment for 15 min. A compact ZnO ETL (~40 nm) was first deposited onto the substrate by spin-coating at 3000 rpm for 30 s, followed by annealing at 150°C for 30 min. Subsequently, the Cs_2NaBiI_6 precursor solution was spin-coated at 4000 rpm for 40 s and annealed at 200°C for 10 min. The film thickness was approximately 300–350 nm. Finally, a NiO HTL (~30 nm) was deposited, and the devices were completed by thermal evaporation of Cu electrodes (~80 nm) under high vacuum.

2.3 Device fabrication

The final device architecture was FTO/ZnO/Cs_2NaBiI_6/NiO/Cu. For each doping concentration (0%, 1%, 3%, 5%), 25 independent devices were fabricated, resulting in a total of 100 devices. This large sample set ensured statistical reproducibility of photovoltaic parameters. Device active area was defined as 0.1 cm² using a shadow mask during Cu deposition.

2.4 Characterization

The structural properties of the films were examined using X-ray diffraction (XRD, Bruker D8 Advance, Cu K-α radiation, λ=1.5406 Å) operated at 40 kV and 40 mA. Surface morphology was investigated by field-emission scanning electron microscopy (FE-SEM). Transmission electron microscopy (TEM) was used to confirm microstructural features. Optical absorption spectra were measured with a UV-Vis spectrophotometer (Shimadzu UV-2600).

Current density–voltage (J-V) characteristics of the solar cells were recorded under simulated AM 1.5G sunlight (100 mA cm^{-2}) using a solar simulator (Newport Oriel, Class AAA) calibrated with a certified Si reference cell. The J-V scans were performed in both forward and reverse directions at a scan rate of 10 mV s^{-1}. Device statistics were reported as mean ± standard deviation based on 25 devices per doping level. Steady-state photocurrent measurements were also performed at the maximum power point for representative devices. Low-light (200-600 W m^{-2}) and external quantum efficiency (EQE) measurements were not conducted in this study and are acknowledged as limitations.

3. RESULTS AND DISCUSSION

3.1 Structural properties

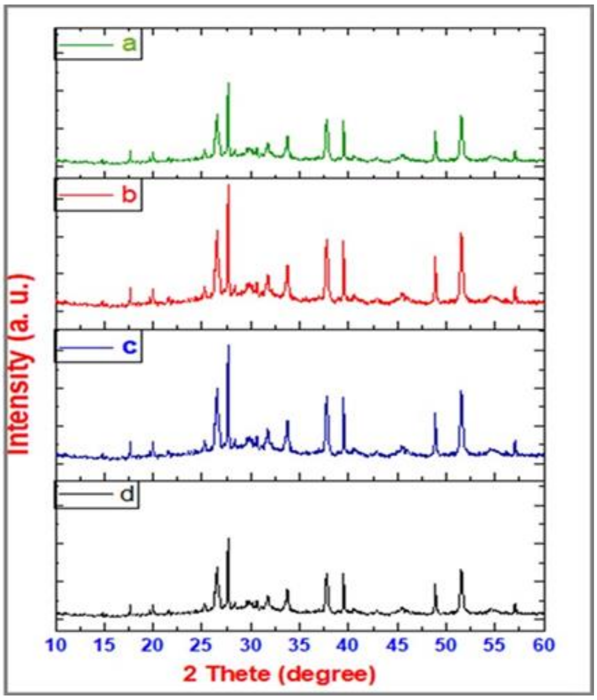

Figure 1. XRD patterns of Cs_2NaBiI_6 films with various Mg doping concentrations: (a) undoped, (b) 1% Mg, (c) 3% Mg, and (d) 5% Mg

In Figure 1, X-ray diffraction (XRD) patterns of pristine and Mg^{2+}-doped Cs_2NaBiI_6 thin films reveal the formation of a well-crystallized double perovskite phase without detectable secondary impurities. The diffraction peaks of all samples are indexed to the cubic perovskite structure, confirming phase purity. Upon Mg^{2+} incorporation, a slight shift of the main peaks toward higher angles is observed, which is consistent with the substitution of smaller Mg^{2+} ions (0.72 Å) relative to Na^{+} (1.02 Å) or Bi^{3+} (1.03 Å). This lattice contraction indicates successful incorporation of Mg^{2+} into the perovskite lattice, inducing minor distortion and thereby tuning the crystal symmetry.

The improved peak intensity and narrowing of the full width at half maximum (FWHM) further suggest enhanced crystallinity, particularly at the optimal doping level of 3%. Excessive doping (≥5%) leads to broadening of peaks, implying increased structural disorder due to oversaturation of Mg^{2+} in the host lattice.

3.2 Morphological analysis

Surface morphology investigated by Field Emission scanning electron microscopy (FE-SEM) demonstrates significant differences between pristine and Mg^{2+}-doped films. The undoped Cs_2NaBiI_6 layer shows a granular texture with voids and incomplete grain coverage. With Mg^{2+} doping up to 3%, the grains become more compact and interconnected, resulting in a denser film with fewer pinholes. This microstructural improvement is expected to suppress non-radiative recombination pathways at grain boundaries. At higher Mg^{2+} content (5%), however, the films exhibit irregular morphology and the reappearance of voids, consistent with the XRD results that indicate reduced crystallinity. While atomic force microscopy (AFM) or grain size distribution analysis was not performed, the FE-SEM evidence qualitatively demonstrates the beneficial role of moderate Mg^{2+} incorporation. This limitation is acknowledged as part of the experimental scope (Figure 2). However, the lack of AFM analysis or quantitative grain size distribution remains a limitation, and such data would strengthen the morphological discussion.

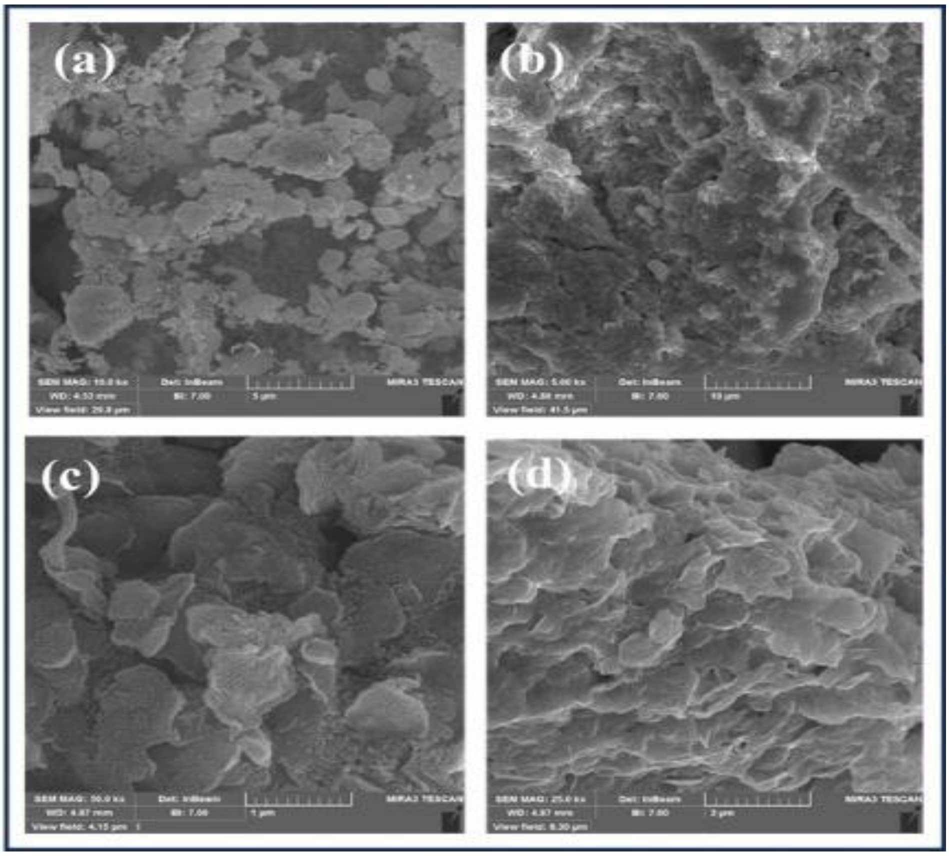

Figure 2. FE-SEM micrographs of Cs_2NaBiI_6 films with varying Mg doping levels: (a) undoped, (b) 1% Mg, (c) 3% Mg, and (d) 5% Mg

3.3 Nanostructure analysis (TEM)

In Figure 3, TEM images provided further insight into the nanoscale morphology. The undoped film displayed poorly defined nanocrystals with heterogeneous size distribution, indicating uncontrolled nucleation. At 1% Mg^{2+}, particles became slightly more uniform, but significant variation remained. The 3% Mg^{2+}-doped sample exhibited well-defined nanocrystals with sharp lattice fringes and a narrower size distribution, confirming enhanced crystallinity and more ordered growth. At 5% doping, particle agglomeration and reduced lattice coherence were observed, suggesting structural strain and possible secondary phase formation.

3.4 Optical properties

UV–visible absorption spectra indicate that pristine Cs_2NaBiI_6 has an absorption onset around 1.8 eV, in agreement with literature reports. Doping with Mg^{2+} induces a red-shift in the absorption edge, reducing the effective bandgap to ~1.65 eV at 3% doping (Figure 4). This shift can be attributed to enhanced orbital overlap between Bi–I states due to lattice distortion caused by Mg^{2+} incorporation, as supported by theoretical models reported for similar systems. Excessive doping again reverses this trend, leading to slight bandgap widening. The improved optical absorption at moderate doping aligns well with the observed crystallinity and morphology trends.

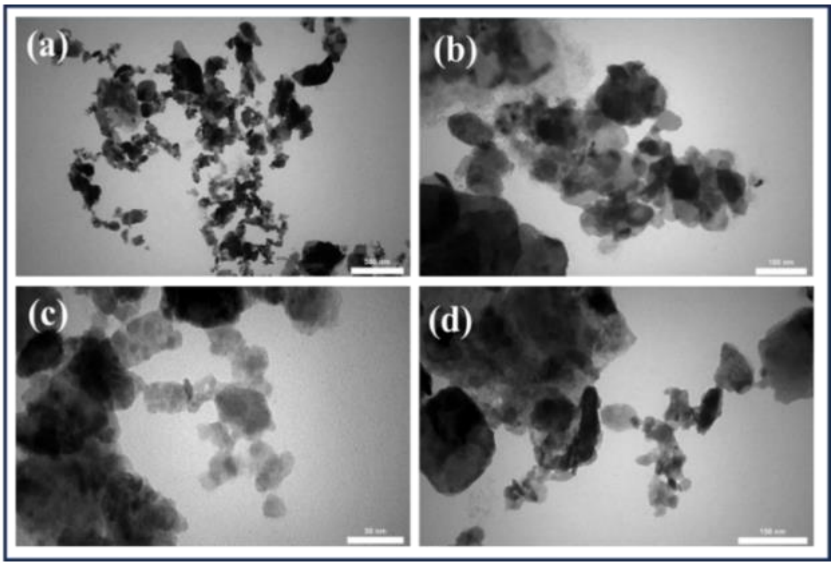

Figure 3. TEM images of Cs_2NaBiI_6 nanoparticles: (a) undoped, (b) 1% Mg, (c) 3% Mg, and (d) 5% Mg

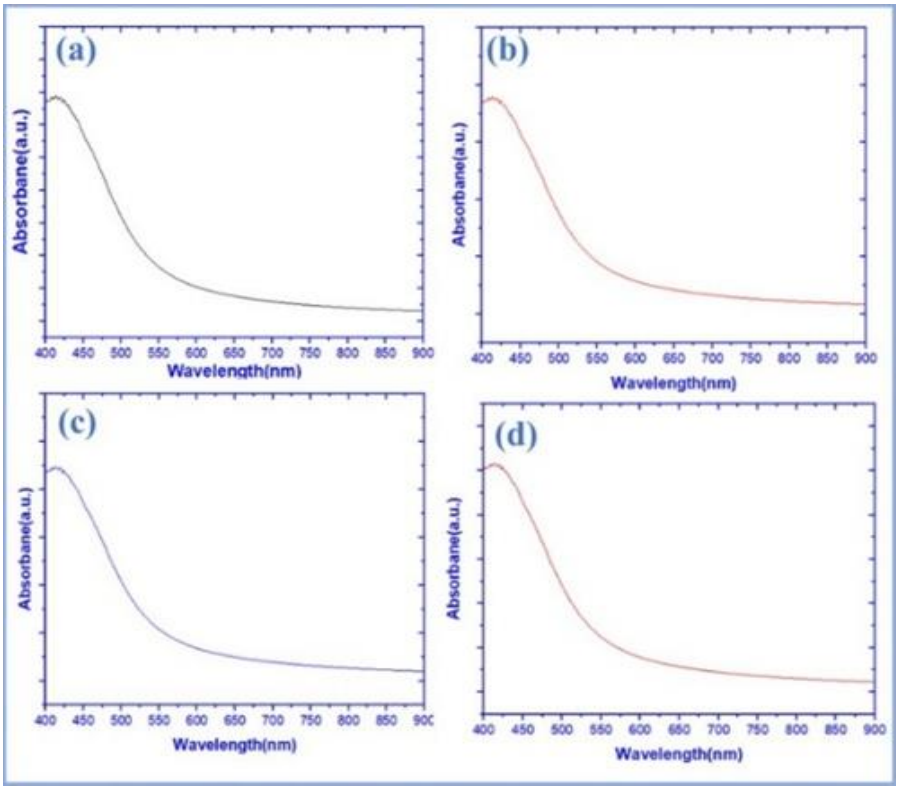

Figure 4. UV–Vis absorption spectra of Cs_2NaBiI_6 films with different Mg doping levels: (a) undoped, (b) 1% Mg, (c) 3% Mg, and (d) 5% Mg

3.5 Photovoltaic performance

The photovoltaic properties of devices fabricated with the structure FTO/ZnO/Cs_2NaBiI_6/NiO/Cu were systematically evaluated under AM 1.5G illumination. A total of 100 devices were fabricated (25 for each doping concentration: 0%, 1%, 3%, 5%) to ensure reproducibility (Figure 5). The average device parameters are summarized in Table 1 as mean ± standard deviation. Pristine devices exhibit modest performance, with an average power conversion efficiency (PCE) of ~0.62%. With 3% Mg^{2+} incorporation, the average PCE increases to 1.22%, representing nearly a two-fold improvement. This enhancement arises mainly from higher short-circuit current density (Jsc) and improved fill factor (FF), attributed to enhanced charge extraction due to improved morphology and reduced trap density. At 5% doping, performance decreases, consistent with structural and morphological degradation.

The differences in open-circuit voltage (Voc) between groups are relatively small, reflecting limited changes in energetic alignment. Champion device performance was also highlighted, with the best-performing 3% Mg^{2+}-doped device showing a PCE of 1.34% and superior steady-state photocurrent compared to the undoped reference. These results demonstrate that moderate Mg^{2+} incorporation enhances device performance consistently across the sample set.

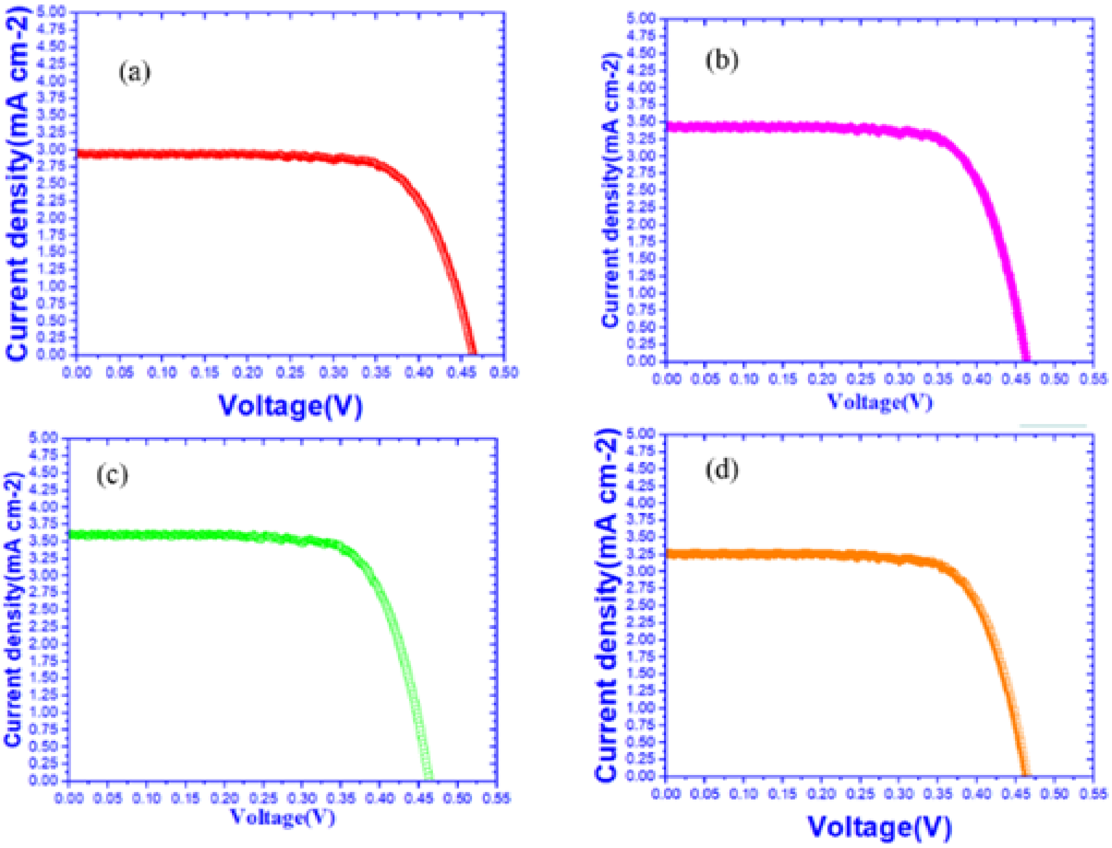

Figure 5. J-V curves of Cs_2NaBiI_6-based solar cells with Mg doping levels of (a) 0%, (b) 1%, (c) 3%, and (d) 5%

Table 1. Photovoltaic parameters of Cs_2NaBiI_6-based solar cells with different Mg^{2+} doping concentrations (mean ± SD, *N*=25 devices per group)

	Perovskite Comp.	ETL	HTL	Metal	Jsc (mA/cm²)	Voc (V)	FF	PCE (%)
A1	Cs_2NaBiI_6 (undoped)	ZnO	NiO	Cu	2.98 ± 0.12	0.45 ± 0.01	0.726 ± 0.015	0.62 ± 0.05
A2	Cs_2NaBiI_6 – Mg 1%	ZnO	NiO	Cu	3.30 ± 0.15	0.47 ± 0.01	0.735 ± 0.018	0.91 ± 0.07
A3	Cs_2NaBiI_6 – Mg 3% (opt.)	ZnO	NiO	Cu	3.80 ± 0.16	0.43 ± 0.02	0.749 ± 0.017	1.22 ± 0.09
A4	Cs_2NaBiI_6 – Mg 5%	ZnO	NiO	Cu	3.20 ± 0.14	0.43 ± 0.01	0.659 ± 0.020	0.76 ± 0.08

3.6 Interpretation of structure–property relationship

The observed improvements in crystallinity, morphology, and optical absorption directly correlate with enhanced photovoltaic performance at optimal doping. However, the relatively modest PCE, despite a narrowed bandgap and improved film quality, suggests that non-radiative recombination remains significant. The absence of time-resolved photoluminescence (TRPL) or impedance spectroscopy in this study limits the direct identification of carrier lifetimes and recombination pathways. We attribute the performance gap to residual defect-mediated recombination, particularly at grain boundaries and interfaces, and emphasize that further optoelectronic characterization should be pursued in future work. This limitation is partly due to the absence of TRPL or impedance spectroscopy measurements, which should be addressed in future work.

3.7 Stability and practical implications

Devices retained stable performance after extended ambient storage, but quantitative data such as retention percentage after a defined time period (e.g., >90% PCE after 500 hours) would improve the reliability of the stability claim.

4. CONCLUSION

In summary, we have systematically investigated the impact of Mg^{2+} incorporation on the structural, morphological, optical, and photovoltaic properties of the lead-free double perovskite Cs_2NaBiI_6. XRD and FE-SEM results confirmed that moderate Mg^{2+} doping (3%) enhances crystallinity and film compactness, accompanied by a reduction in optical bandgap (~1.65 eV) and improved light absorption. These modifications translated into reproducible photovoltaic performance, with the average power conversion efficiency increasing from 0.62% for pristine devices to 1.22% at optimal doping, supported by data from 100 devices (25 per group). At higher doping concentrations, performance degradation was observed, consistent with structural disorder and poor morphology.

The correlation between improved material properties and enhanced device performance underscores the effectiveness of cation doping as a strategy for tuning iodide-based double perovskites. Nevertheless, the modest efficiency despite bandgap narrowing indicates that non-radiative recombination remains a limiting factor. While advanced optoelectronic characterization (e.g., TRPL or impedance spectroscopy) was not performed in this study, our results strongly suggest that defect-mediated carrier losses play a key role and should be addressed in future investigations.

Importantly, Cs_2NaBiI_6 demonstrates superior environmental stability compared to bromide-based analogues, making it attractive for niche applications such as indoor photovoltaics and durable low-power devices, where stability is prioritized over peak efficiency. This work provides new insights into doping strategies for iodide-based lead-free double perovskites and offers a foundation for further development of environmentally benign, stable photovoltaic materials.

ACKNOWLEDGMENT

This research is supported by the Department of Physics, College of Science, University of Thi-Qar, as part of a Master graduation requirements.

REFERENCES

[1] Zhang, B.W., Lin, C.H., Nirantar, S., Han, E.Q., Zhang, Y., Wang, Z., Wang, L. (2024). Lead-free perovskites and metal halides for resistive switching memory and artificial synapse. Small Structures, 5(6): 2300524. https://doi.org/10.1002/sstr.202300524

[2] Tailor, N.K., Listorti, A., Colella, S., Satapathi, S. (2023). Lead-free halide double perovskites: Fundamentals, challenges, and photovoltaics applications. Advanced Materials Technologies, 8(1): 2200442. https://doi.org/10.1002/admt.202200442

[3] Wu, Y., Li, X., Zeng, H. (2021). Lead-free halide double perovskites: Structure, luminescence, and applications. Small Structures, 2(3): 2000071. https://doi.org/10.1002/sstr.202000071

[4] Igbari, F., Wang, Z.K., Liao, L.S. (2019). Progress of lead-free halide double perovskites. Advanced Energy Materials, 9(12): 1803150. https://doi.org/10.1002/aenm.201803150

[5] Raheem, Z., Abdulsada, R., Kadhim, S.B., AbdulAlmohsin, S.M., Abdulaali, H.S. (2023). High efficiency (22.46) of solar cells based on perovskites. University of Thi-Qar Journal of Science, 10(2): 187-191. https://doi.org/10.32792/utq/utjsci/v10i2.1140

[6] Noel, N.K., Stranks, S.D., Abate, A., Wehrenfennig, C., Guarnera, S., Haghighirad, A.A., Snaith, H.J. (2014). Lead-free organic–inorganic tin halide perovskites for photovoltaic applications. Energy & Environmental Science, 7(9): 3061-3068. https://doi.org/10.1039/C4EE01076K

[7] Zhang, S., Liu, G., Teng, B., Ji, S. (2025). Lead-free metal halide double perovskites–From crystal design to optoelectronic applications. CrystEngComm, 27(21): 3416-3432. https://doi.org/10.1039/D5CE00310E

[8] Ahmed, S., Gondal, M.A., Alzahrani, A.S., Parvaz, M., Ahmed, A., Hussain, S. (2024). Recent trends and challenges in lead-free perovskite solar cells: A critical review. ACS Applied Energy Materials, 7(4): 1382-1397. https://doi.org/10.1021/acsaem.3c02327

[9] Abdulsada, Z.R., AbdulAlmohsin, S.M. (2021). High efficiency solar cells base on organic-inorganic perovskites materials. University of Thi-Qar Journal of Science, 8(2): 23-29. https://doi.org/10.32792/utq/utjsci.v8i2.808

[10] Verma, A.A., Dwivedi, D.K. (2025). Performance benchmarking of lead-free double perovskites: Design optimization and comparative analysis of inorganic Cs2BX6 (B= Sn, Pd; X= Br, I) perovskites for efficient PSCs. Journal of Inorganic and Organometallic Polymers and Materials, pp. 1-17. https://doi.org/10.1007/s10904-025-03983-2

[11] Shah, S.Z.A., Niaz, S., Nasir, T., Sifuna, J. (2022). Eco-friendly bismuth based double perovskites $X_2NaBiCl_6$ (X= Cs, Rb, K) for Optoelectronic and Thermoelectric Applications: A First-Principles Study. arXiv preprint arXiv:2208.04123. https://doi.org/10.48550/arXiv.2208.04123

[12] Hussein, A.A. (2020). Enhancement efficiency of active layer P3HT:POT:DBSA/PCBM photoactive solar cell device. University of Thi-Qar Journal of Science, 7(2): 90-94. https://doi.org/10.32792/utq/utjsci/v7i2.722

[13] Grandhi, G.K., Hardy, D., Krishnaiah, M., Vargas, B., Al-Anesi, B., Suryawanshi, M.P., Vivo, P. (2024). Wide-bandgap perovskite-inspired materials: Defect-driven challenges for high-performance optoelectronics. Advanced Functional Materials, 34(50): 2307441. https://doi.org/10.1002/adfm.202307441

[14] Tabassum, M., Zia, Q., Zhou, Y., Reece, M.J., Su, L. (2021). A review on advances in doping with alkali metals in halide perovskite materials. SN Applied Sciences, 3(12): 888. https://doi.org/10.1007/s42452-021-04877-x

[15] Datta, A.K., Hossain, M.K., Rahman, M.S., Paramasivam, P., El-Marghany, Mishra, V.K. (2025). DFT insights into bandgap engineering of lead-free LiMCl3 (M= Mg, Be) halide perovskites for optoelectronic device applications. Scientific Reports, 15(1): 6944. https://doi.org/10.1038/s41598-025-90621-z

[16] Traore, A., Li, X., Molang, C. (2024). Investigation of the structural, electronic, optical, and interface properties of the two-dimensional Dion Jacobson perovskite BDA (MA) Mg 2 I 7 for lead-free solar cells using density functional theory. In 2024 4th International Conference on New Energy and Power Engineering (ICNEPE), Guangzhou, China, pp. 150-154. https://doi.org/10.1109/ICNEPE64067.2024.10860596

[17] Kumar, V., Kathiravan, A., Jhonsi, M.A. (2024). Beyond lead halide perovskites: Crystal structure, bandgaps, photovoltaic properties and future stance of lead-free halide double perovskites. Nano Energy, 125: 109523. https://doi.org/10.1016/j.nanoen.2024.109523

[18] Bi, J., Lv, H., Wang, H., Du, L., Liu, Y., Shen, Y., Ning, W. (2025). Bandgap engineering of lead-free double perovskites for efficient photocatalysis. Nanoscale, 17: 14263-14270. https://doi.org/10.1039/D5NR01676B

[19] Li, X., Shi, J., Chen, J., Tan, Z., Lei, H. (2023). Lead-free halide double perovskite for high-performance photodetectors: Progress and perspective. Materials, 16(12): 4490. https://doi.org/10.3390/ma16124490

[20] Tang, H., Xu, Y., Hu, X., Hu, Q., Chen, T., Jiang, W., Jiang, W. (2021). Lead-free halide double perovskite nanocrystals for light-emitting applications: Strategies for boosting efficiency and stability. Advanced Science, 8(7): 2004118. https://doi.org/10.1002/advs.202004118

[21] Jindal, R., Tripathi, A., Mohan, C., Garg, A., Varma, R.S. (2024). Lead-free halide double perovskites for

sustainable environmental applications. Chemical Physics Impact, 9: 100770. https://doi.org/10.1016/j.chphi.2024.100770

[22] Shi, X., Hou, C., Wang, S., Wang, B. (2025). A strategy for boosting luminescence in lead-free double perovskites via passivation-induced surface engineering. Applied Surface Science, 707: 163618. https://doi.org/10.1016/j.apsusc.2025.163618

[23] Bai, Z.J., Yang, A.J., Tian, S., Chen, L., Wang, B.H., Hu, B., Yin, S.F. (2023). Multi-dimensional lead-free hybrid double perovskite toward efficient and stable photocatalytic selective oxidation of toluene. Chemical Engineering Science, 282: 119334. https://doi.org/10.1016/j.ces.2023.119334

[24] Yu, W., Zou, Y., Wang, H., Qi, S., Wu, C., Guo, X., Xiao, L. (2024). Breaking the bottleneck of lead-free perovskite solar cells through dimensionality modulation. Chemical Society Reviews, 53(4): 1769-1788. https://doi.org/10.1039/D3CS00728F

[25] Singh, S., Nayak, P.K., Tretiak, S., Ghosh, D. (2023). Composition dependent strain engineering of lead-free halide double perovskite: Computational insights. The Journal of Physical Chemistry Letters, 14(42): 9479-9489. https://doi.org/10.1021/acs.jpclett.3c02249